PERGAMON

Atmospheric Environment 36 (2002) 5185–5196

ATMOSPHERIC ENVIRONMENT

www.elsevier.com/locate/atmosenv

FTIR measurements of functional groups and organic mass in aerosol samples over the Caribbean

Steven F. Maria[a], Lynn M. Russell[a,*], Barbara J. Turpin[b], Robert J. Porcja[b]

[a] *Department of Chemical Engineering, Princeton University, Princeton, NJ 08544, USA*
[b] *Department of Environmental Science, Rutgers University, New Brunswick, NJ 08854, USA*

Received 1 April 2002; accepted 3 August 2002

Abstract

An aircraft-based aerosol concentrator consisting of three virtual impactors in series has been used to collect particles for Fourier transform infrared (FTIR) transmission spectroscopy on stretched Teflon filters. Submicron atmospheric aerosol samples were collected near St. Croix aboard the National Center for Atmospheric Research C-130 aircraft during the passing efficiency of a low-turbulence inlet project. FTIR identified sulfate, ammonium, silicate, and organic functional groups, and a four-solvent rinsing procedure separated these functional groups into fractions of increasing hygroscopicity. The Caribbean aerosols contained 0.01–1.6 μg m^{-3} of Si, indicative of African mineral dust at all altitudes, with higher Al/Ca ratios in the boundary layer. Organic compounds were present in high and low dust conditions with estimated total organic mass varying from 0.8–4 μg m^{-3} during the project. Aliphatic carbon and carbonyl carbon were quantified at concentrations of up to 4 and 0.8 μg m^{-3}, respectively, and were summed to calculate organic carbon and organic mass (OM) concentrations. Sequential solvent rinsing with repeated FTIR analysis revealed that 60–90% of OM in the free troposphere was hygroscopic, with hydrophobic organic compounds accounting for 20–50% of OM in the marine boundary layer.

Keywords: Organic aerosol; Particle concentrator; Organic polarity; Organic solubility; Dust aerosol

1. Introduction

Organic vapors and products of their photochemical oxidation form new particles or may condense onto pre-existing particles. Partly as a result of this vapor-to-particle conversion, the atmosphere contains aerosol particles composed of complex mixtures of water-soluble inorganic salts, insoluble mineral dust, and carbonaceous material. This carbonaceous fraction includes organic compounds ranging from very soluble to insoluble, plus elemental carbon (Jacobson et al., 2000; Saxena and Hildemann, 1997).

The solubility of the carbonaceous fraction affects the hygroscopic growth and deliquescence behavior of atmospheric particles (Ming and Russell, 2001). Commonly used thermal organic carbon (OC) measurements give none of the information on organic functional group composition that is required to estimate this effect. The resulting dearth of information may cause general circulation models to underestimate the organic particles that serve as cloud condensation nuclei, leading to underpredictions of OC wet deposition by factors of 2–7 (Cooke et al., 1999). The calculation of aerosol optical properties from compositional measurements also requires an estimate of OC hygroscopicity, as optical properties depend on particle size. Uncertainties of up to 15% in the derived extinction coefficient and 18% in the derived scattering coefficient have been reported to be caused by the assumption that all OC is hydrophobic (Collins et al., 2000). These uncertainties can be particularly large in the free troposphere, where

*Corresponding author.
E-mail address: lrussell@princeton.edu (L.M. Russell).

1352-2310/02/$ - see front matter
PII: S1352-2310(02)00654-4

recent aircraft-based measurements found OC mass fractions from 50–90% (Novakov et al., 1997).

OC functional group composition and solubility can be used to predict thermodynamic equilibrium based on organic composition (Ming and Russell, 2001). This work describes a new technique for measuring concentrations and solubilities of organic functional groups (carbonyl and methyl) and inorganic ions (SO_4^{2-}, NH_4^+, SiO_4^{4-}) in submicron aerosol samples collected from aircraft during the passing efficiency of the low-turbulence inlet (PELTI) field project.

2. Experimental procedure

During the PELTI experiment in June of 2000, submicron aerosol samples were collected near St. Croix from the NCAR C-130 aircraft. A three-stage particle concentrator (3SPC) consisting of three slit virtual impactors (Sioutas et al., 1994) in series was used to increase the concentration of the sample aerosol stream by up to a factor of 19 prior to collection on 37 mm stretched Teflon filters (Teflo 1 μm, Pall Corp., Ann Arbor, MI). FTIR and XRF analysis allowed for the identification of inorganic and organic functional groups as well as elemental composition.

2.1. Particle concentrator

A schematic of the 3SPC, following the design of Sioutas et al. (1994), is shown in Fig. 1 (P. Koutrakis, Harvard University). The 3SPC improved the time resolution of measurements and allowed for the use of a small sample stream flow rate ($2\,l\,min^{-1}$) that minimized the pressure drop across the filter, avoided sampling artifacts, facilitated flow control, and reduced pumping load at altitude. For an ambient submicron aerosol concentration of $4\,\mu g\,m^{-3}$, it would take 20 h to collect a 10 μg sample on a 37 mm diameter filter ($2\,l\,min^{-1}$; $64\,cm\,s^{-1}$ face velocity) without concentration. The 3SPC reduces the required sampling time to a little over 1 h.

Sample air from the NCAR C-130 Community Aerosol Inlet (CAI) (Blomquist et al., 2001) was pulled at a rate of $180\,l\,min^{-1}$ through a 1.06 μm cutoff impactor and then through the 3SPC. Efficiency curves for both the 1.06 μm cutoff impactor and the 3SPC are shown in Fig. 2. The concentration enhancement factor of laboratory-generated sodium chloride aerosol particles (Fig. 2b) was measured by comparing particle number size distributions upstream and downstream of the 3SPC using a differential mobility analyzer (TSI, Model 3071) for 0.1–0.9 μm diameter particles (Hoppel, 1978) and an aerodynamic particle sizer (TSI, Model 3320) for 0.55–20.0 μm diameter particles (Brockmann et al., 1988). The 3SPC performance is size dependent,

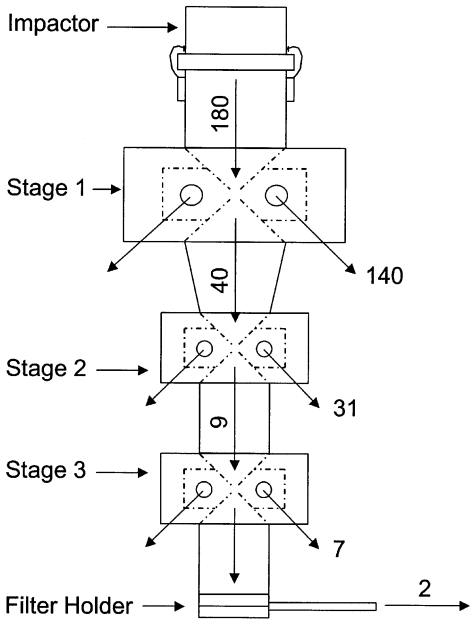

Fig. 1. Schematic of the three stage particle concentrator with flows labelled in LPM.

with a maximum concentration factor of 27 occurring at 0.5–0.7 μm. Each virtual impactor stage removes 78% of the carrier gas in the major flow while retaining 22% of the carrier gas and more than 50% of particles greater than 0.3 μm diameter in the sample stream (minor flow). This is equivalent to a per stage concentration factor of 2.3 for 0.3 μm diameter particles and 3.0 for 0.6 μm diameter particles.

All flows were maintained constant volumetrically by manually setting mass flow controllers (Teledyne-Hastings HFC-202 and HFC-203) to account for changes in inlet temperature and pressure. The 3SPC performance was checked on the aircraft by a comparison of particle size distributions measured with externally mounted optical probes to the particle mass loadings of the filter samples at 40% relative humidity, as shown in Fig. 3. Sampled submicron mass from size distribution estimates agreed within 5% of gravimetric measurements for both sea-salt and dust aerosol, consistent with the 3SPC efficiency curve under atmospheric conditions. The mass-average concentration enhancement factor determined for each submicron size distribution varied from 13 to 19 depending on the mass mean size of the ambient aerosol collected for each sample. Fig. 3 demonstrates size distributions with mass-average concentration factors of 15 for the sea-salt sample and 19 for the dust sample. For the sea-salt sample, the concentration factor drops to 50% of the mass-average concentration factor at 0.2 and 1.3 μm diameter, compared to 50% cutoff diameters of 0.3 and 1.2 μm

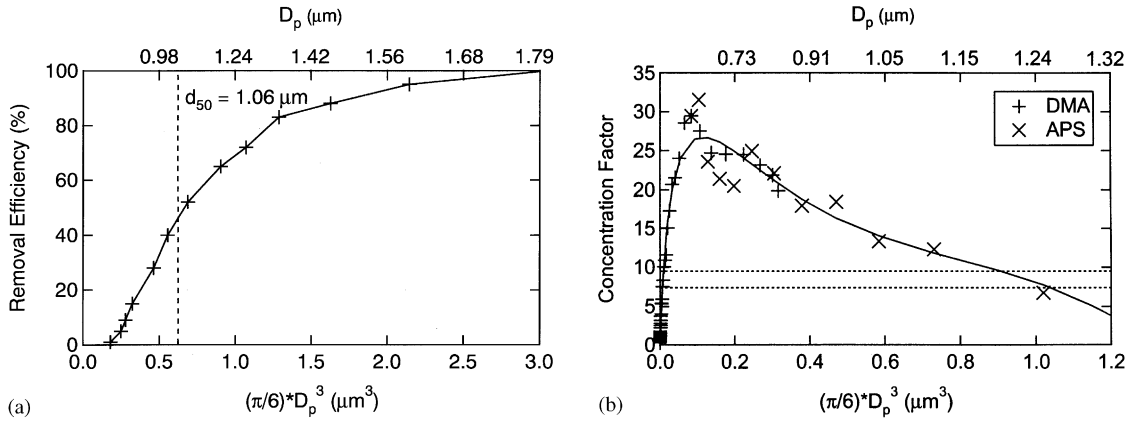

Fig. 2. 3SPC removal efficiency and concentration factor as a function of particle volume, measured using NaCl aerosol. (a) Collection efficiency of the 1.06 μm impactor at the inlet of the 3SPC, reported as the percentage of particles of each size that are removed from the sample stream. (b) Performance of the complete 3SPC, including the impactor. The concentration factor is defined as the aerosol mass concentration at the filter divided by the ambient aerosol mass concentration at the inlet. Dotted lines show the 50% cutoff diameters for mass-average concentration factors of 15 (sea-salt) and 19 (dust) corresponding to the size distributions shown in Fig. 3.

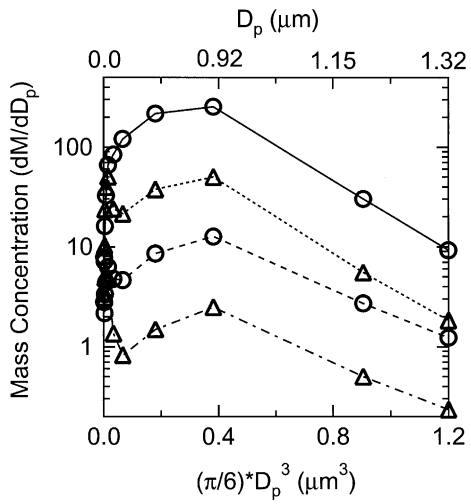

Fig. 3. Comparison of measured and estimated submicron particle mass distributions as functions of particle volume. Ambient PCASP submicron size distributions for sea-salt at 300 m on 16 July 2000 (dash-dotted line with triangles, with an integrated submicron mass of 2.0 μg m^{-3}) and for dust at 2800 m on 21 July 2000 (dashed line with circles, with an integrated submicron mass of 6.8 μg m^{-3}). Estimated sample stream size distributions at the Teflon filter for the sea-salt (dotted line with triangles) and dust (solid line with circles) were calculated by weighting the ambient size distribution by the 3SPC calibration curve in Fig. 2b. Sample stream submicron mass is 30 μg m^{-3} from size distribution estimates as compared to gravimetrically determined mass concentrations of 28 ± 5 μg m^{-3} for the sea-salt sample, and 130 μg m^{-3} for the dust sample that had a gravimetrically determined concentration of 124 ± 20 μg m^{-3}.

for the dust sample. Uncertainties in the CAI inlet efficiency and PCASP size distributions (Blomquist et al., 2001; Collins et al., 2000; Liu and Daum, 2000) add an approximately 15% error to all calculated mass-average concentration factors.

During the PELTI project, 30 filter samples and 88 blanks were collected for flight legs in the marine boundary layer and in free tropospheric air masses originating in Northern Africa. Flight legs ranged in length from 20 to 145 min. Table 1 shows that no detectable peaks were observed on any downstream blanks, consistent with previous studies that did not find significant organic artifacts on Teflon filters (Turpin et al., 1994).

2.2. FTIR spectroscopy and rinsing procedure

Field samples were analyzed using a Mattson Research Series 100 FTIR Spectrometer with a deuterated triglycine sulfate (DTGS) detector and a He–Ne laser. FTIR spectra were collected in transmission mode for each filter by averaging 200 absorbance scans at wavenumbers from 400 to 4000 cm^{-1} with a resolution of 4 cm^{-1}. Teflon filters were scanned prior to use, and the resulting spectra were subtracted from scans after sampling to obtain the absorbance of the sampled aerosol. Filter support rings were etched to ensure that alignment was maintained during consecutive scans.

Ammonium, carbonate, and many organic compounds absorb radiation between 1420 and 1440 cm^{-1}. To differentiate between overlapping peaks and to characterize the solubility of organic components, we carried out sequential rinsing of each sample with

Table 1
Absorbance of blanks and average project errors

	Absorbance per filter				FTIR	XRF
	Clean room blanks[a] (70)[b]	Handling blanks[c] (9)	Downstream blanks[d] (9)	Min. detectable peak	error (%)	error (%)
SO_4^{2-}	0.078±0.138	0.083±0.102	0.073±0.059	0.04	24±13	23±11
NH_4^+	0.047±0.079	0.054±0.075	0.051±0.040	0.05	26±12	—
SiO_4^{4-}	0.021±0.043	0.019±0.032	0.023±0.019	0.02	15±14	13±8
OC	0.188±0.318	0.188±0.243	0.183±0.171	0.17	48±20	—

[a] Loaded and stored in the on-site clean room, with one blank per sample filter and additional blanks for assessing variability.
[b] Number of each filter type is in parenthesis.
[c] Loaded as samples but with no flow pulled through them.
[d] Placed behind sample filters during sampling in flight.

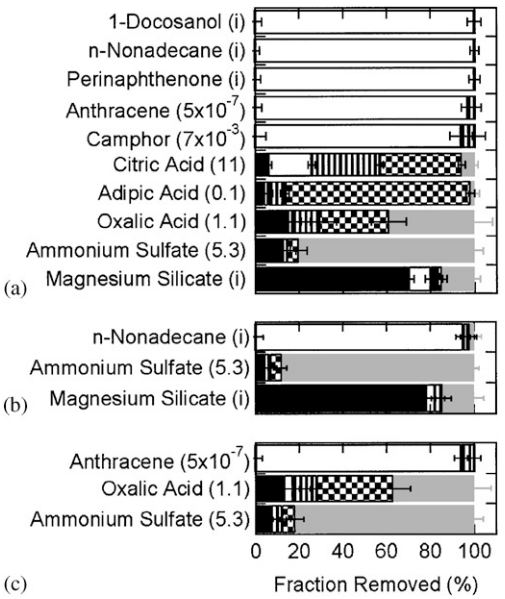

Fig. 4. Measured rinse removal characteristics of some typical organic and inorganic species in the atmosphere, with results from (a) pure species, (b) a mixture of ammonium sulfate, magnesium silicate, and nonadecane, and (c) a mixture of ammonium sulfate, oxalic acid, and anthracene. Bars represent (from left to right) the fraction remaining on the filter after all rinsing was completed (black) and the fractions removed in hexane (white), dichloromethane (striped), acetone (checkered), and water (grey). Error bars indicate uncertainty in the FTIR measurements. Numbers in parentheses indicate water solubility in M, with the letter i indicating a water solubility of less than 5×10^{-7} M.

solvents of increasing polarity: hexane, dichloromethane (DCM), acetone, and water (Blando et al., 1998; Carlton et al., 1999). At 1420–1440 cm^{-1}, the organic fraction is removed in hexane, DCM or acetone while the ammonium fraction is removed in water and the carbonate fraction remains on the filter after all rinsing is complete.

The rinsing method used 1 ml of each of the organic solvents and 5 ml of water. Gentle vacuum flow was used to pull the organic solvents across the filter as the solvents were dropped onto the sample. The samples were rinsed with water by placing 5 ml of water on each sample and allowing the water to sit for 1 min before being poured off. The fractions removed in each stage of this solvent-rinsing procedure for laboratory-generated samples of magnesium silicate, ammonium sulfate, oxalic acid, citric acid, adipic acid, perinaphthenone, 1-docosanol, n-nonadecane, camphor, and anthracene are shown in Fig. 4.

2.3. XRF analysis

XRF was performed on the sample filters to quantify elements heavier than sodium, including iron, silicon, sulfur, calcium, chlorine, and vanadium (Chester Lab-Net, Tigard, OR). XRF detection limits reflect the signal-to-noise ratio for each element, and reported errors include the detection limit plus a 5% calibration uncertainty as well as spectral overlap uncertainties when a secondary line from one element overlaps the primary line from another element.

3. Mass quantification

GRAMS/32 software (Thermo Galactic, Salem, NH) was used to subtract pre-scans from post-scans, to correct for the scan-to-scan shift in the baseline absorbance, and to integrate spectral peaks as shown in Fig. 5. Absorbance peaks associated with sulfate, ammonium, silicate, and aliphatic carbon were identified in the majority of samples.

Fig. 6 shows spectra taken after each solvent rinse, in addition to the difference in sequential rinses indicating

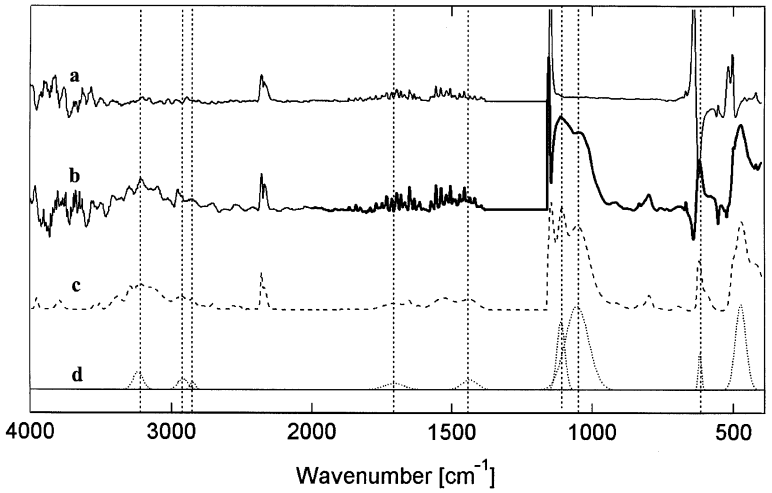

Fig. 5. Example PELTI spectrum and curve-fitting analysis: (a) FTIR spectrum of a blank Teflon filter, (b) FTIR spectrum of aerosol collected at 40 m from 1635 to 1744 GMT on 9 July 2000 during PELTI research flight 2, (c) peak-fitting spectrum showing the sum of all integrated peak sizes, and (d) individual peaks derived using the peak-fitting routine. The dotted lines represent (from left to right) ammonium (3220 cm^{-1}), C–H (2920 cm^{-1}), C–H (2850 cm^{-1}), C=O (1720 cm^{-1}), ammonium (1437 cm^{-1}), sulfate (1110 cm^{-1}), silicate (1035 cm^{-1}), and sulfate (618 cm^{-1}).

the fraction removed in each rinse. The sharp peaks at 2850, 2920 and 2960 cm^{-1} in Fig. 6d and e reveal a clear C–H signature dominated by hydrophobic alkanes that are removed by hexane. Carbonyl carbon (1720 cm^{-1}) was usually below detection because it was too small to be clearly distinguished from water interference at 1600–1700 cm^{-1}.

Ammonium interference was removed from the aliphatic carbon absorbance measurement by scaling an ammonium sulfate reference spectrum to the ammonium absorbance at 3238 cm^{-1} and then subtracting the ammonium reference spectrum before integration of the aliphatic peaks. Up to 80% of the remaining absorbance was removed in the hexane, DCM, and acetone rinses (with up to 40% removed in hexane alone), showing removal of hydrophobic compounds that cannot be attributed to interference from ammonium. Teflon interference also was removed from the sulfate peak at 618 cm^{-1} for each sample spectrum by scaled subtraction of the corresponding blank spectrum. The functional groups that were identified after these corrections, along with their corresponding absorption frequencies and detection limits, are shown in Table 2.

Table 2
Peaks used in FTIR quantification of aerosol functional groups

Functional group	Quantified frequencies[a] (cm^{-1})	Calibrated absorbances (abs^{-1})[b]	Detection limit (μg cm^{-2})
SO_4^{2-}	580–635	0.41	0.72
HSO_4^-	580–635	0.41	0.72
SiO_4^{4-}	1035	0.011	0.09
NH_4^+	1435	0.14	0.11
C–H	2850–2920	1.04[c]	1.15
C=O	1640–1850	0.061[d]	0.51

[a] Determined using previously published aerosol spectra (Allen et al., 1994) and laboratory-generated submicron aerosol standards.

[b] abs = absorptivity = peak area (in absorbance units) per micromole of functional group. This calibration of absorptivity is specific to our spectrometer.

[c] Determined from *n*-nonadecane and citric acid standards.

[d] Determined from citric acid, adipic acid, and oxalic acid standards.

3.1. Functional group quantification

Linear relationships between mass and infrared absorbance for ammonium and sulfate on Teflon filters have been reported previously by McClenny et al. (1985). This technique quantifies moles of bonds from absorbance, using the measured absorption per mole of each component from laboratory-generated standards. With our spectrometer, the absorbance of ammonium sulfate, citric acid, adipic acid, and magnesium silicate varied linearly with the number of moles of bonds and mass loading, independent of mixture composition, as shown in Fig. 7. For each standard a linear fit had a correlation above $R^2 = 0.88$, with slopes in Table 2. Adipic and citric acid were used as model compounds for calibration because they are representative of the multifunctional acids that have been measured in

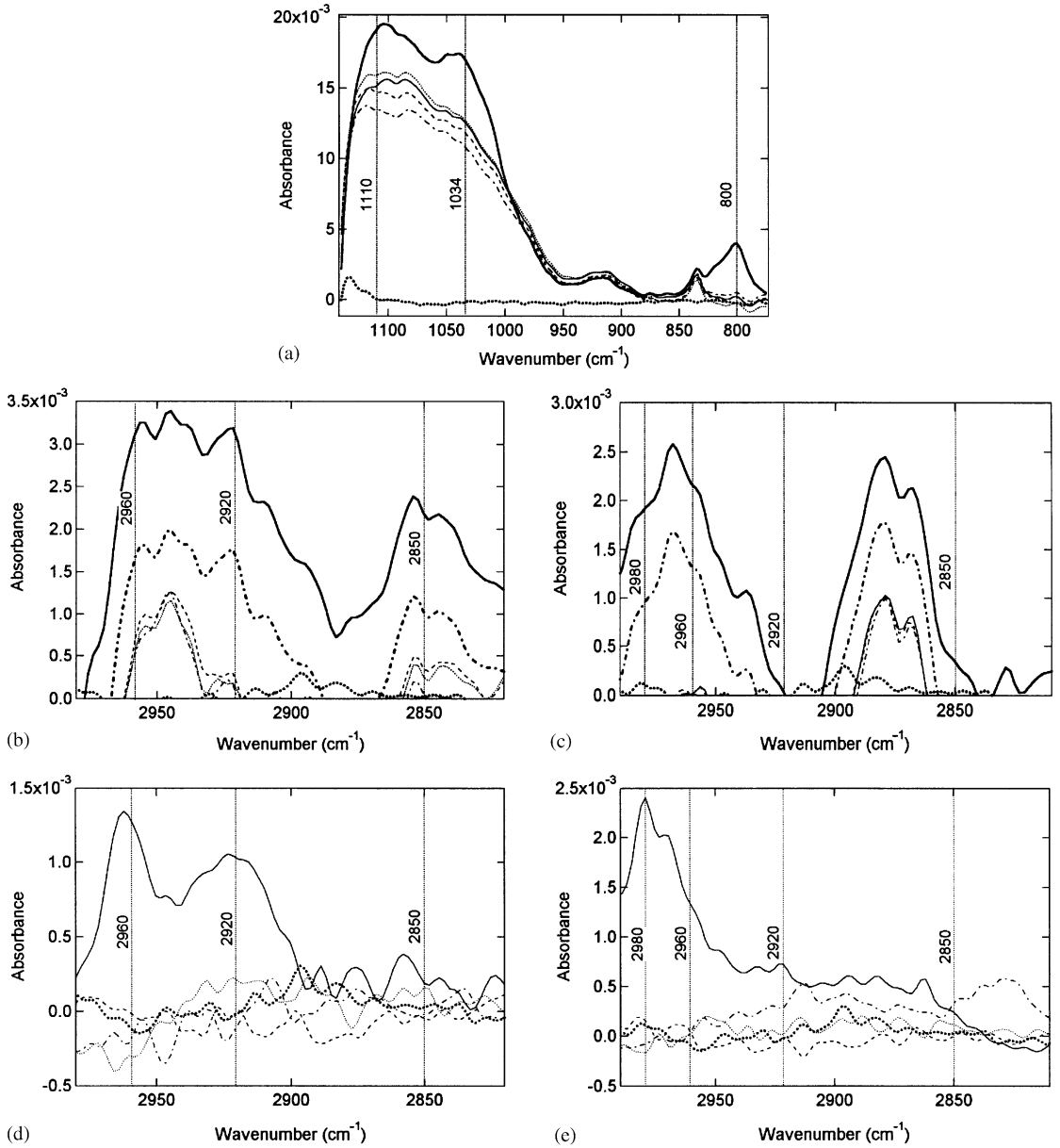

Fig. 6. Details of PELTI spectra and their changes with rinsing: (a) a sulfate peak at 1100 cm^{-1} (overlapping with quartz and silicate absorbances), a silicate peak at 1034 cm^{-1}, and an unidentified peak at 800 cm^{-1}; (b), (c) characteristic C–H absorbances; (d), (e) difference spectra showing the absorbance removed in each solvent rinse. Figs. (a), (b), and (d) are for the 40 m sample of Fig. 5, while (c) and (e) are for a 6000 m free tropospheric sample collected on 23 July 2000 at 1622–1831 GMT. In panels (a)–(c) the original sample spectrum is shown as a bold solid line, the spectra after rinsing with hexane as a thin solid line, dichloromethane as a dotted line, acetone as a dashed line, and water as a dot–dashed line, and the corresponding blank spectrum as a thick dotted line. In panels (b) and (c) the spectrum after correcting for ammonium interference is shown as a bold dash–dotted line. In panels (d) and (e) spectra removed by each solvent are shown (hexane as a thin solid line, dichloromethane as a dotted line, acetone as a dashed line, and water as a dot-dashed line), and the corresponding blank spectrum is shown as a thick dotted line.

ambient fine aerosols in marine conditions (Duce et al., 1983). Two multi-component mixtures were also checked to see if cross-compound interactions would cause non-linearities in the absorbance signal. No changes in absorptivity were seen in the mixtures as illustrated in Fig. 7.

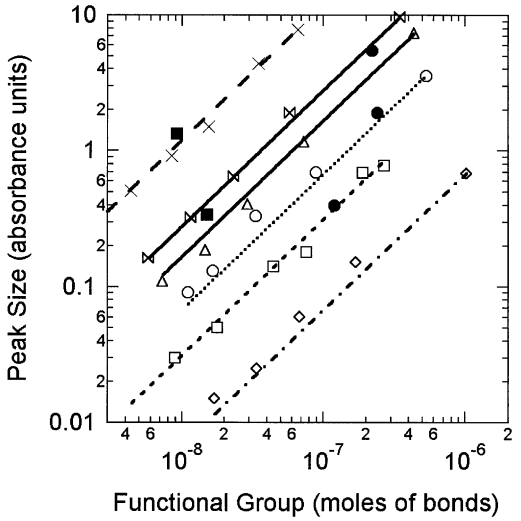

Fig. 7. FTIR response for laboratory generated aerosol of several species in varying sample amounts. Open circles are NH_4^+ (ammonium) from $(NH_4)_2SO_4$ aerosol, open squares are SO_4^{2-} (sulfate) from $(NH_4)_2SO_4$ aerosol, triangles are C=O (carbonyl) from citric acid aerosol, hourglasses are C=O (carbonyl) from adipic acid aerosol, diamonds are C–H carbon from citric acid aerosol, and crosses are SiO_4^{4-} (silicate) from magnesium silicate. Filled squares show the absorbance behavior of a 50% magnesium silicate and 50% adipic acid mixture, and filled circles indicate mixture behavior of a 50% ammonium sulfate and 50% adipic acid mixture. All mixture data points correspond to the functional group with the curve fit that they are nearest to. Lines indicate best-fit linear correlations to the data.

Two estimates were used to quantify the range and uncertainty for these measurements: (1) twice the standard deviation of the absorption values associated with blank filters, accounting for spectral noise as well as contamination associated with filter preparation and handling, and (2) a visual determination of the minimum peak size that could be distinguished from spectral noise. The larger of the two quantities was used as the detection limit and error for each functional group, as listed in Table 1. For 1 h concentrated filter samples, FTIR errors are smaller than 20% for ambient sulfate concentrations greater than 0.45 μg m^{-3}, for ammonium loadings greater than 0.07 μg m^{-3}, and for aliphatic carbon loadings greater than 0.72 μg m^{-3}.

FTIR sulfate and XRF S are weakly correlated with $R^2 = 0.42$. The presence of non-sulfate sulfur contained in organosulfur compounds is indicated by hexane-soluble absorbance peaks at 800 cm^{-1} (consistent with methane sulfonic acid (MSA)) that are present in most of the samples in which the XRF S exceeded the FTIR sulfate S. XRF Si measurements were consistently higher than FTIR silicate Si. To explain this, the 1090 and 1010 cm^{-1} peaks after water rinsing were used to identify absorbances associated with insoluble quartz and kaolinite species. The resulting total of all Si species from FTIR correlates weakly with the XRF Si with $R^2 = 0.44$, and the slope of 1.8 indicates that some Si-containing species are present that were not detected by FTIR.

The average error in the FTIR data quantified by this direct calibration was less than that of the ratio method (Cliff and Lorimer, 1972; Blando et al., 2001) by a factor of two, because the error in the ratio method includes the uncertainties of our calibrated FTIR absorbance ratios and the XRF measurements as well as the comparability of XRF-measured S or Si with FTIR-measured S or Si. The presence of significant non-sulfate sulfur and non-silicate silicon (in the form of MSA, quartz, and kaolinite, as discussed above) made use of sulfate or silicate as an internal standard inappropriate. The ratio method had errors of 52–93% whereas the FTIR direct calibration method average error was 31%.

3.2. Organic mass estimates

OC mass and total organic mass (OM) were estimated assuming that there were two moles of C–H bonds per mole of aliphatic carbon and one mole of C=O bonds per carbonyl carbon:

$$\mathrm{OC} = (0.5 \times [\text{moles C}-\mathrm{H}] \times [12\ \mathrm{g\ mol^{-1}}]) + ([\text{moles C}=\mathrm{O}] \times [12\ \mathrm{g\ mol^{-1}}]), \quad (1)$$

$$\mathrm{OM} = (0.5 \times [\text{moles C}-\mathrm{H}] \times [14\ \mathrm{g\ mol^{-1}}]) + ([\text{moles C}=\mathrm{O}] \times [28\ \mathrm{g\ mol^{-1}}]). \quad (2)$$

As defined, OC includes carbon mass only and OM includes carbon, hydrogen, and oxygen. This definition is equivalent to a carbon mass to organic compound mass conversion factor of 1.2 for aliphatic carbon and 2.3 for carbonyl carbon. These conversion factors span the range suggested by Turpin and Lim (2001).

The aliphatic carbon conversion factor assumes that all C–H is in the form CH_2, an assumption with an error of less than 12% if the average organic molecule size is a saturated carbon chain of four or more carbons. This assumption is appropriate for long-chain condensed organic compounds measured in the atmosphere by chromatography (Matsumoto and Hanya, 1980). To quantify the maximum error in this assumption, we consider an extremely polluted organic aerosol in which 25% of OC is in the form of oxalic acid (with mass-to-carbon ratio of 3.8 g gC^{-1}) and the remaining 75% of OC is a more typical urban organic composition (with mass-to-carbon ratio of 1.6 g gC^{-1}), resulting in an actual mass-to-carbon ratio in the mixture of 2.2 g gC^{-1}. The FTIR method using Eq. (2) underestimates OM by 17% to give an effective mass-to-carbon ratio of

1.8 g gC^{-1}, whereas the "urban aerosol" 1.6 mass-to-carbon ratio of Turpin and Lim (2001) underpredicts by 26%.

The presence of organonitrates, organosulfates or alcohols would result in an underestimate of organic compound mass. However, nitrogen-containing organic functional groups were not identified in any PELTI samples and are not a large component of marine aerosol (Chester and Stoner, 1974). MSA and alcohols are also minor marine aerosol components, representing $<5\%$ of the identified organic carbon. We therefore do not expect any significant OM underestimates for the PELTI project.

4. Discussion

Isentropic back-trajectories from the PELTI sampling region using the NOAA HYSPLIT4 model (Draxier and Hess, 1998) indicate that all sampled air masses originated over Africa and had been transported over the Atlantic for 5 to 6 days before we sampled them in the Caribbean (Garrett et al., 2002). The boundary layer height averaged 1800 m based on temperature and relative humidity profiles. Vertical distributions of FTIR and XRF-measured species are shown in Fig. 8, and project-average summary statistics are given in Table 3. Concentrations of ammonium, sulfate, and silicate ions were larger in the free troposphere than in the boundary layer, while organic carbon showed no clear trend with altitude.

Elemental compositions and Fe, Al, and Si ratios provide indicators of African mineral dust. Si dominates the elemental composition of free tropospheric samples and appears in low-altitude samples at concentrations that are comparable to S and Cl. The high Al/Ca ratio indicates a large mineral dust aerosol fraction (Perry et al., 1997). Measured organic carbon concentrations varied from 1–4 μg m^{-3} for samples that were above detection limit. The highest organic concentrations (4 μg m^{-3}) correspond to NaCl submicron mass fractions of $>40\%$, but organics were measured in concentrations as high as 2 μg m^{-3} even when dust comprised more than 80% of the submicron mass.

The aerosol number-to-volume ratio (N/V), calculated using PCASP and differential mobility analyzer (DMA) size distribution measurements from 0.06 to 1.8 μm diameter, has been shown to vary linearly with the aerosol organic mass fraction (Hegg and Russell, 2000). This linear relationship may be caused by secondary sulfate production, which lowers both the organic mass fraction and the N/V ratio (Hegg and Russell, 2000). PELTI size distributions using the PCASP and a radial differential mobility analyzer (RDMA) from 0.06 to 1.8 μm diameter show that N/V increases as organic mass fraction increases, although the fit has an R^2 value of only 0.37 as illustrated in Fig. 9. This value is comparable to the R^2 value of 0.41 reported for the TARFOX and ACE 2

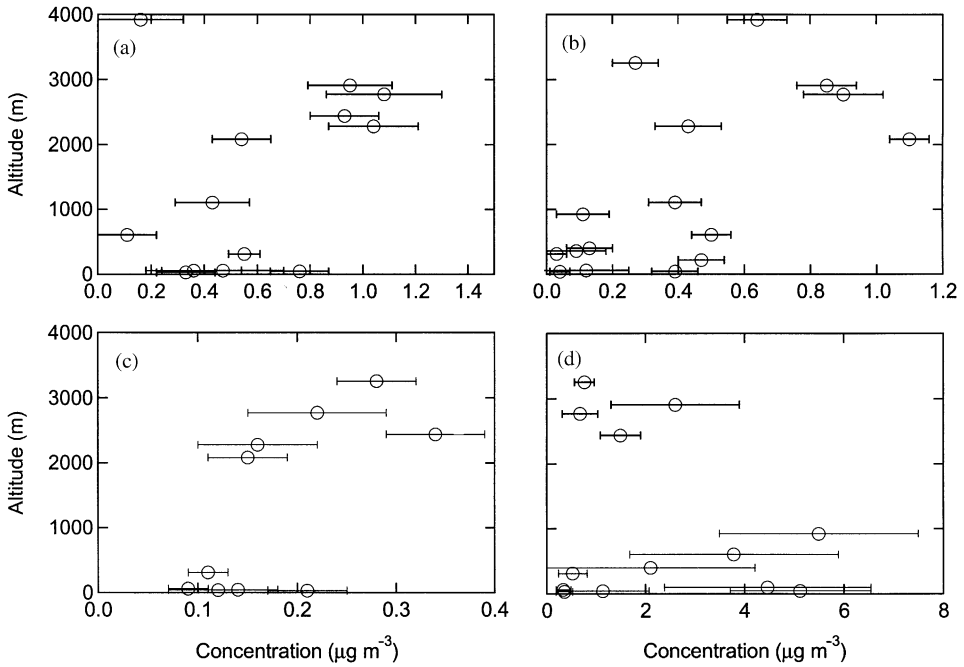

Fig. 8. FTIR vertical distributions of (a) sulfate, (b) silicate, (c) ammonium, and (d) organic carbon.

Table 3
Project average and variability of PELTI submicron particle composition by FTIR and XRF

Functional group	Altitude range					
	0–50 m		50–1800 m		> 1800 m	
	Average ($\mu g\ m^{-3}$)	St.Dev. ($\mu g\ m^{-3}$)	Average ($\mu g\ m^{-3}$)	St.Dev. ($\mu g\ m^{-3}$)	Average ($\mu g\ m^{-3}$)	St.Dev. ($\mu g\ m^{-3}$)
C=O (FTIR)	0.35	NA	0.17	NA	0.70	0.09
C–H (FTIR)	2.19	2.57	3.24	2.02	2.45	2.40
NH_4^+ (FTIR)	0.14	0.05	0.11	NA	0.20	0.10
SO_4^{2-} (FTIR)	0.48	0.20	0.36	0.23	0.78	0.36
S (XRF)	0.12	0.07	0.18	0.06	0.29	0.19
SiO_4^{4-} (FTIR)	0.18	0.18	0.24	0.20	0.70	0.31
Si (XRF)	0.10	0.06	0.29	0.21	1.29	0.46
Al (XRF)	0.03	0.01	0.11	0.09	0.59	0.34
Cl (XRF)	0.14	0.04	0.09	0.06	0.08	0.03
K (XRF)	0.02	0.01	0.04	0.01	0.11	0.04
Ca (XRF)	0.03	0.01	0.06	0.02	0.21	0.08
Ti (XRF)	0.02	0.02	0.01	0.004	0.04	0.01
Cr (XRF)	BDL	NA	0.004	0.002	0.008	0.004
Mn (XRF)	BDL	NA	0.006	0.002	0.008	0.003
Fe (XRF)	0.04	0.02	0.11	0.03	0.41	0.15
Cu (XRF)	0.005	NA	0.003	NA	0.005	NA
Ga (XRF)	0.004	NA	0.01	0.003	0.01	NA
Sn (XRF)	0.02	NA	0.04	0.02	0.07	0.03
Pb (XRF)	0.01	NA	0.01	0.004	0.02	NA

NA = not applicable, indicating that fewer than two measured values were above the detection limit. BDL = all values below detection limit.

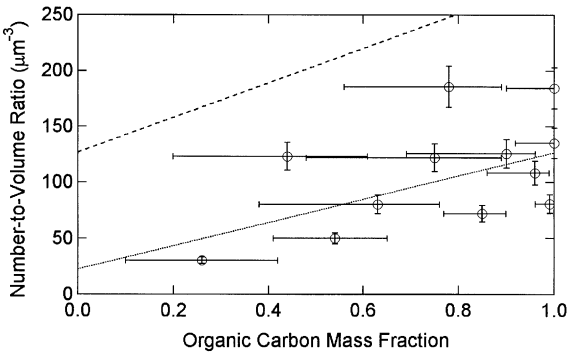

Fig. 9. Number-to-volume ratio and the OC mass fraction, defined as the FTIR-measured OC mass divided by the total gravimetric mass. Markers show individual samples, the dotted line shows the best fit linear correlation to the data ($N/V = 104 \times$ OC mass fraction $+ 23$, $R^2 = 0.37$), and the dashed line shows the fit for the combined TARFOX-ACE 2 data sets ($N/V = 155 \times$ OC mass fraction $+ 127$, $R^2 = 0.41$) (Hegg and Russell, 2000).

data sets (Hegg and Russell, 2000). The slope of 104 for the linear fit is similar to the value of 155 ± 44 reported by Hegg and Russell (2000). However, the intercepts differ because the average N/V ratio for the PELTI project is $107 \pm 49\ \mu m^{-3}$, smaller than the value of $168 \pm 51\ \mu m^{-3}$ found by Hegg and Russell (2000) in the more polluted North Atlantic studies. The N/V ratio for the boundary layer is $131 \pm 39\ \mu m^{-3}$, indicative of a local source of submicron particles. The free troposphere has an N/V ratio of $48 \pm 18\ \mu m^{-3}$, consistent with the large average size and small number of submicron dust particles.

4.1. Solubility of organic and inorganic fractions

The effect of solvent rinsing on the PELTI sample of Fig. 5 is shown in Fig. 6, with spectral changes after each rinse separating the identified FTIR functional group absorbances into fractions of increasing water solubility. The organic C–H peaks at 2850 and 2920 cm^{-1} were removed largely in hexane and partly in acetone, indicating hydrophobic compounds. Peaks at 1040 and 800 cm^{-1} were removed in the hexane rinse, consistent with organosulfur compounds such as MSA.

Project-average rinse results for the marine boundary layer and free troposphere are shown in Table 4. Carbonyl carbon, detectable in only two PELTI samples, was removed partially in DCM and completely in acetone. Aliphatic carbon in the troposphere was less soluble in hexane and more soluble in acetone than aliphatic carbon in the marine boundary layer. This trend held for individual samples in Fig. 10, with smaller

Table 4
Solubility of chemical components measured by FTIR

	Percentage removed[a]							
	Boundary layer (<1800 m)				Free troposphere (> 1800 m)			
Rinse	SO_4^{2-}	NH_4^+	SiO_4^{4-}	C–H	SO_4^{2-}	NH_4^+	SiO_4^{4-}	C–H
Hexane	2±3	16±20	8±7	35±6	7±17	11±16	4±8	19±7
DCM	6±9	6±7	12±15	9±19	4±6	13±16	8±10	3±5
Acetone	0±1	18±12	9±11	9±19	4±4	1±3	0±2	31±18
Water	52±18	28±10	1±2	34±25	57±27	36±28	26±32	40±29
Residual	37±15	29±12	70±5	13±7	26±15	35±24	62±21	7±5

[a] Percentages shown are for the entire project data set, and represent the average fraction of each sample that was removed during each rinsing stage, as well as the standard deviations.

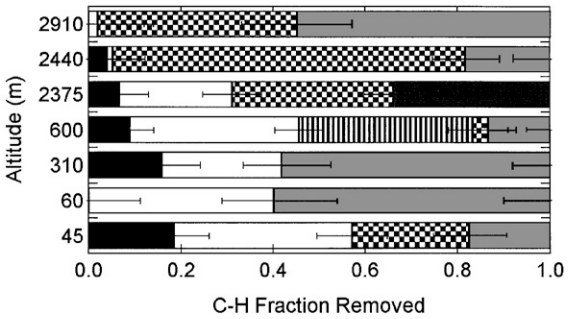

Fig. 10. Removal characteristics for the C–H absorbance peak, showing the fractions removed in hexane (white), dichloromethane (striped), acetone (checkered), and water (gray), and the fraction remaining on the filter after all rinsing was completed (black). Each horizontal bar represents one filter sample. Error bars indicate uncertainty in the FTIR measurements.

hexane-soluble C–H fractions above the boundary layer. Below 1800 m, an average of 35% of the identified C–H was hydrophobic, with a range of 20–50%. Above 1800 m, 2 of 3 samples had no hydrophobic fraction, and 60–90% of C–H was soluble in water. These results suggest that the organic carbon in the free troposphere is more water-soluble, because organic standards removed by hexane have water solubilities of <0.01 M (Fig. 4) and water-soluble standards are removed by either acetone or water.

In the marine boundary layer, the observed OC solubility behavior is consistent with a model organic aerosol composition of 30% *n*-nonadecane, 20% citric acid, and 50% oxalic acid. In the free troposphere , an organic composition of 0–10% *n*-nonadecane, 40% adipic acid, and 50–60% oxalic acid would be consistent with the observed rinsing behavior. These relatively hygroscopic model compositions provide more accurate estimates of the activation potential of organic aerosol within a cloud, allowing us to avoid underestimating OC wet deposition (Cooke et al., 1999). The uncertainty in aerosol scattering and extinction coefficients derived from composition measurements can also be reduced by $\sim$10% for OM mass fractions of 50–90% (Collins et al., 2000), with the assumption that our measured OM solubilities and resulting hygroscopic growth factors are accurate to within $\sim$20%.

Residual values of sulfate, ammonium, and silicate show more than 15% of the measured groups remained after all four solvent rinses. This result is expected for silicates as many silicate compounds are insoluble in water and organic solvents. The large residuals in the ammonium and sulfate measurements result from a combination of the compounded error in each post-rinse scan of smaller absolute absorbances (and larger relative errors) as well as spectral interference by dust components with overlapping absorbance peak locations (carbonate at 1433 cm^{-1} and soil at 550 cm^{-1}).

5. Conclusions

FTIR spectroscopy with an aircraft-based aerosol sampling system showed total identified submicron aerosol functional group concentrations varying from 0.4–6.0 μg m^{-3}. Organic carbon was identified in samples composed largely of sea-salt as well as in samples dominated by dust. A four-solvent rinsing procedure separated functional groups into fractions based on solubility, showing larger fractions of water-soluble organics at high altitudes.

The assumption that OC is 100% hydrophobic (Collins et al., 2000) or 50% hydrophobic (Cooke et al., 1999) neglects important spatial variations in OC properties. Incorporation of measured organic hygroscopicity into models will result in larger predicted OC concentrations in cloud droplets. Uncertainties in

scattering and extinction coefficients calculated from aerosol composition are also reduced.

Acknowledgements

This research was supported by NSF Grants ATM-0002035 and ATM-9732949 and by ONR grants N00014-97-1-0673 and N00014-98-0565. We gratefully acknowledge the help of Adam Reff in designing the aerosol generation system we used for collection of reference compounds. We also appreciate the advice and help of Petros Koutrakis, Stephen Ferguson, and Ilias Kavouras of the Harvard School of Public Health in the design and assembly of the 3SPC. We are grateful to Krista Laursen, Barry Huebert, Graeme Christianson, Elizabeth Fetter, and the NCAR Research Aviation Facility for their help in the field.

References

Allen, D.T., Palen, E.J., Haimov, M.I., Hering, S.V., Young, J.R., 1994. Fourier transform infrared spectroscopy of aerosol collected in a low pressure impactor (LPI/FTIR): method development and field calibration. Aerosol Science and Technology 21, 325–342.

Blando, J.D., Porcja, R.J., Li, T.H., Bowman, D., Lioy, P.J., Turpin, B.J., 1998. Secondary formation and the Smoky Mountain organic aerosol: an examination of aerosol polarity and functional group composition during SEAVS. Environmental Science and Technology 32, 604–613.

Blando, J.D., Porcja, R.J., Turpin, B.J., 2001. Issues in the quantitation of functional groups by FTIR spectroscopic analysis of impactor-collected aerosol samples. Aerosol Science and Technology 35, 899–908.

Blomquist, B.W., Huebert, B.J., Howell, S.G., Litchy, M.R., Twohy, C.H., Schanot, A., Baumgardner, D., Lafleur, B., Seebauch, R., Laucks, M.L., 2001. An evaluation of the community aerosol inlet for the NCAR C-130 research aircraft. Journal of Atmospheric and Oceanic Technology 32, 1387–1397.

Brockmann, J.E., Yamano, N., Lucero, D., 1988. Calibration of the aerodynamic particle sizer 3310 (APS-3310) with polystyrene latex monodisperse spheres and oleic-acid monodisperse particles. Aerosol Science and Technology 8, 279–281.

Carlton, A.G., Turpin, B.J., Johnson, W., Buckley, B.T., Simcik, M., Eisenreich, S.J., Porcja, R.J., 1999. Microanalysis methods for characterization of personal aerosol exposures. Aerosol Science and Technology 31, 66–80.

Chester, R., Stoner, J.H., 1974. The distribution of particulate organic carbon and nitrogen in some surface waters of the world ocean. Marine Chemistry 2, 263–275.

Cliff, G., Lorimer, G.W., 1972. Quantitative analysis of thin metal foils using EMMA-4 (electron microscope-microanalyzer) ratio technique. Proceedings of the Fifth European Congress on Electron Microscopy, pp. 140–141.

Cooke, W.F., Liousse, C., Cachier, H., 1999. Construction of a $1^\circ \times 1^\circ$ fossil fuel emission data set for carbonaceous aerosol and implementation and radiative impact in the ECHAM4 model. Journal of Geophysical Research 104, 22137–22162.

Collins, D.R., Jonsson, H.H., Seinfeld, J.H., Flagan, R.C., Gasso, S., Hegg, D.A., Russell, P.B., Schmid, B., Livingston, J.M., Ostrom, E., Noone, K.J., Russell, L.M., Putaud, J.P., 2000. In situ aerosol-size distributions and clear-column radiative closure during ACE-2. Tellus, Series B 52, 498–525.

Draxier, R.R., Hess, G.D., 1998. An overview of the $HYSPLIT_4$ modelling system for trajectories, dispersion and deposition. Australian Meteorological Magazine 47, 295–308.

Duce, R.A., Mohnen, V.A., Zimmerman, P.R., Grosjean, D., Cautreels, W., Chatfield, R., Jaenicke, R., Ogren, J.A., Pellizzari, E.D., Wallace, G.T., 1983. Organic material in the global troposphere. Reviews of Geophysics and Space Physics 21, 921–952.

Garrett, T.J., Russell, L.M., Ramaswamy, V., Maria, S.F., Huebert, B.J., 2002. Microphysical and radiative evolution of aerosol plumes over the tropical North Atlantic ocean. Journal of Geophysical Research, in press.

Hegg, D.A., Russell, L.M., 2000. An analysis of processes determining the number-to-volume relationship for submicron aerosol in the Eastern Atlantic. Journal of Geophysical Research 105, 15321–15328.

Hoppel, W.A., 1978. Determination of the aerosol size distribution from the mobility distribution of the charged fraction of aerosols. Journal of Aerosol Science 9, 41–54.

Jacobson, M.C., Hansson, H.C., Noone, K.J., Charlson, R.J., 2000. Organic atmospheric aerosols: review and state of the science. Reviews of Geophysics 38, 267–294.

Liu, Y.G., Daum, P.H., 2000. The effect of refractive index on size distributions and light scattering coefficients derived from optical particle counters. Journal of Geophysical Research 31, 945–957.

Matsumoto, G., Hanya, T., 1980. Organic constituents in atmospheric fallout in the Tokyo area. Atmospheric Environment 14, 1409–1419.

McClenny, W.A., Childers, J.W., Rohl, R., Palmer, R.A., 1985. FTIR transmission spectroscopy for the nondestructive determination of ammonium and sulfate in ambient aerosols collected on Teflon filters. Atmospheric Environment 19, 1891–1898.

Ming, Y., Russell, L.M., 2001. Predicted hygroscopic growth of sea salt aerosol. Journal of Geophysical Research 106, 28259–28274.

Novakov, T., Hegg, D.A., Hobbs, P.V., 1997. Airborne measurements of carbonaceous aerosols on the East Coast of the United States. Journal of Geophysical Research 102, 30023–30030.

Perry, K.D., Cahill, T.A., Eldred, R.A., Dutcher, D.D., Gill, T.E., 1997. Long-range transport of North African dust to the eastern United States. Journal of Geophysical Research 102, 11225–11238.

Saxena, P., Hildemann, L.M., 1997. Water absorption by organics: survey of laboratory evidence and evaluation of UNIFAC for estimating water activity. Environmental Science and Technology 31, 3318–3324.

Sioutas, C., Koutrakis, P., Burton, R.M., 1994. Development of a low cutpoint slit virtual impactor for sampling ambient fine particles. Journal of Aerosol Science 25, 1321–1330.

Turpin, B.J., Huntzicker, J.J., Hering, S.V., 1994. Investigation of organic aerosol sampling artifacts in the Los Angeles basin. Atmospheric Environment 28, 3061–3071.

Turpin, B.J., Lim, H.J., 2001. Species contributions to PM2.5 mass concentrations: Revisiting common assumptions for estimating organic mass. Aerosol Science and Technology 35, 602–610.